Commun. Comput. Phys.
doi: 10.4208/cicp.2019.js60.09

Vol. **26**, No. 5, pp. 1617-1630
November 2019

Detecting Particle Clusters in Particle-Fluid Systems by a Density Based Method

Tian Tian[1], Han Wang[2,3], Wei Ge[4,5] and Pingwen Zhang[1,*]

[1] *School of Mathematical Sciences, Peking University, Beijing, 100871, P.R. China.*

[2] *Institute of Applied Physics and Computational Mathematics, Fenghao East Road 2, Beijing 100094, P.R. China.*

[3] *CAEP Software Center for High Performance Numerical Simulation, Huayuan Road 6, Beijing 100088, P.R. China.*

[4] *State Key Laboratory of Multiphase Complex Systems, Institute of Process Engineering, Chinese Academy of Sciences, Beijing 100190, P.R. China.*

[5] *School of Chemical Engineering, University of the Chinese Academy of Sciences (UCAS), Beijing 100049, P.R. China.*

Received 28 February 2019; Accepted (in revised version) 29 April 2019

Abstract. In this paper, the DBSCAN (Density-Based Spatial Clustering of Applications with Noise) method is proposed to detect particle clusters in particle-fluid systems. The particles are grouped in one cluster when they are connected by a dense environment. The parameters that define the dense environment are determined by analyzing the structure of the system, therefore, our approach needs little human intervention. The method is illustrated by identifying the clusters in two kinds of simulation trajectories of different particle-fluid systems. The robustness of cluster identification in terms of statistical properties of clusters in the steady state is demonstrated.

AMS subject classifications: 6207, 70C20, 76T25

Key words: Particle-fluid system, cluster, DBSCAN method.

1 Introduction

The particle-fluid system is widely applied in energy engineering, chemical industry, metallurgy and many other industrial processes [12, 18]. The particle-fluid systems exhibit multi-scale and heterogeneous structures in both time and space. In particular, the

*Corresponding author. *Email addresses:* 1501110025@pku.edu.cn (T. Tian), wang_han@iapcm.ac.cn (H. Wang), wge@ipe.ac.cn (W. Ge), pzhang@pku.edu.cn (P. Zhang)

meso-scale structures, such as clusters and bubbles, have a significant impact on the properties of the system, making it unique in multi-phase systems [7]. For decades, a great effort on the theoretical analysis and experimental research has been devoted to understand how the meso-scale structures change the macroscopic properties of the particle-fluid system [1, 9, 17].

Understanding the self-assembly of particle clusters and the interaction between the clusters and fluid is of particular importance to the study of flow and transport mechanisms in fluidized beds, and is crucial for the operation and design of fluidized bed equipments. The particle cluster is also one of the central concepts in theoretical models that describes the multi-scale structure of the particle-fluid flow system, for example, the energy minimization multi-scale (EMMS) model [5, 6, 8].

Despite the importance of the particle clusters, detecting clusters in experiments or defining cluster from particle trajectories in the numerical simulations is not a trivial task. Soong et al. [14] proposed a criterion to identify clusters in circulating fluidized bed experiments, and this criterion is revised by other groups [13, 15, 16]. A similar idea was followed in these studies: the time-averaged solid concentration plus an integer times the standard deviation of the solid concentration is taken as a threshold; A cluster is identified if the instantaneous solid concentration at the probe tip is larger than the threshold at the same position. The integer in the threshold can be 1, 2, 3 or other numbers depending on the operating condition. The criterion can be easily applied to define clusters from particle trajectories generated from numerical simulations. A possible implementation partitions the simulation region by a grid, and calculates and the instantaneous solid concentration in each grid cell by counting the number of particles in it. If the concentration satisfies the Soong's criterion, then the grid cell is a part of a cluster. With a larger grid cell the accuracy of the statistical estimation of the concentration is improved, but the resolution of cluster is inevitably decreased. Therefore, the intrinsic uncertainty in defining cluster is the main drawback of this approach. Liu et al. [9] computed the local voidage by the Voronoi tessellation, and then partition the whole heterogeneous structure into a gas-rich phase and a solid-rich dense phase by analyzing the probability distribution of the local voidage. In their approach, clusters can be defined by the collections of inter-connected Voronoi cells, however, this definition is sensitive to the local fluctuation of voidage and the computational cost of Voronoi tessellation is expensive.

In this work, we propose to apply the DBSCAN (Density-Based Spatial Clustering of Applications with Noise) method developed by Ester et al. [4] to identify clusters in the particle trajectories from the numerical simulations of the particle-fluid systems. This approach takes the particle positions as inputs, and defines clusters with rigid and clear mathematical criterion. The DBSCAN model parameters are determined by analyzing the structure of the particle-fluid flow, thus given a criterion identifying the dense phase out of the dilute phase, our approach does not need further parameter tuning and the cluster identification process is automated.

The outline of this paper is as follows: In Section 2, the data generation protocol is described; In Section 3, the cluster identification method DBSCAN method is introduced

and our approach for determining the method parameters is proposed; In Section 4, the results obtained from the algorithm are shown and analyzed; The work is concluded in Section 5.

2 Simulation protocol

To validate our approach, we analyze the data generated by two kinds of numerical simulations of particle-fluid systems, i.e. the direct numerical simulation (DNS) and the energy minimization multi-scale discrete particle method (EMMS-DPM). Next, we briefly introduce the simulation protocols that are used by the simulations.

2.1 DNS simulation protocol

The DNS data were generated by Zhou et al. [17]. The details of their simulation can be find in Ref. [17], here we briefly describe the simulation protocol. The fluid part of the system was carried out by the lattice Boltzmann method (LBM) [10] in a 3-dimensional domain. While the immersed moving boundary (IMB) [11] method was adopted to solve the gas-solid coupling part. Besides, the discrete element method (DEM) [2] was used to deal with the particle-particle collisions. The mesh size is taken to be $\sigma = 3.75\times10^{-6}m$. 28800 particles of diameter of 20σ were randomly put into a simulation domain of size $6144\sigma\times1536\sigma\times128\sigma$. The periodic boundary condition was given for both gas and particles in each direction. The gravitational force $\mathbf{g}_p$ exerted on each particle was of magnitude 3.25×10^{-8}N and the direction was downward along the x-axis. A body force $\mathbf{g}_g$ was exerted on the gas phase to balance the gravitational force $\mathbf{g}_p$ on the particles, so that the net force exerting on the system was 0. The size of the time step was $\Delta t = 5.08\times10^{-8}s$, the data for analysis were sampled at every 5000th step from the 5000th step to the 5.0×10^{6}th step. We denote $\tau = 5000\Delta t$ and investigate the conformation of the system at time interval from $2.54\times10^{-4}s$ to $0.254s$.

2.2 EMMS-DPM simulation protocol

The EMMS-DPM data were generated by Ji Xu et al. in Institute from the Process Engineering, Chinese Academy of Sciences. In their work, a coarse-grained discrete particle method (DPM) defined by the EMMS model was used to simulate a whole circulating fluidized bed (CFB), which is a typical continuous operation device. Some important parameters of the particle and gas used in the EMMS-DPM simulation are listed in Table 1 and Table 2, respectively. In stead of the whole CFB, we identify the particle clusters in the main part of riser, a cylindrical subregion of the CFB system, which is $5.204m$ high with inner diameter of $0.102m$. However, the bottom of the main part of the riser is near the gas inlet, where the properties of the particles may be affected greatly. Therefore, we abandon a small region near the gas inlet, the length of which is 1/72 of the length of the main part of the riser. Then, we choose the particles in the other region of the main part

Table 1: Simulation particle parameters of the lab-scale CFB loop.

Particle diameter, $d_p(\mu m)$	82
Coarse-graining ratio	10
Coarse-grained particle diameter (μm)	820
CGP number	1.27×10^8
Density, ρ_p (kg/m^3)	2450
Time step, $\Delta t(s)$	5×10^{-7}
Solid inventory	90 kg
Young's modulus (Pa)	1×10^6
Poisson's ratio	0.12
Coefficient of friction	0.5
Coefficient of rolling friction	0.1
Characteristic velocity (m/s)	10

Table 2: Simulation gas parameters of the lab-scale CFB loop

Gas phase density (ρ_g) (kg/m^3)	1.1795
Gas phase viscosity (μ_g) $(kg/(m\cdot s))$	1.8872×10^{-5}
Flux at inlet of riser (m^3/h)	110
Flux at left inlet of loop seal (m^3/h)	16.2
Flux at right inlet of loop seal (m^3/h)	5.0
Grid number	261.106
Time step, $\Delta t(s)$	1×10^{-5}
operating pressure (Pa)	1.01×10^5

of the riser to analyze. The region to be analyzed contains about 1×10^7 particles. The snapshots of the particles in that region of the riser are recorded from 32.28s to 32.60s at a time interval of 0.04s.

3 Method

The DBSCAN is a representable cluster identification method based on density. It defines clusters as the largest set of points that are connected by density. It divides the regions with enough high density into clusters, and finds clusters of arbitrary shape only with the spatial data with noise. Given a set of N particles $D=\{x_1,x_2,\cdots,x_N\}$, where x_i denotes the position of the ith particle. The distance between particle i and j are defined by $d_{ij}=\|x_i-x_j+n\|$, where $\|\cdot\|$ denotes the Euclidean distance, and n denotes the simulation cell translation vector to ensure that the distance is computed between nearest periodic images. It is clear that $d_{ij}=d_{ji}$. It is noted that other definitions of "distance" can be adopted directly in the DBSCAN method.

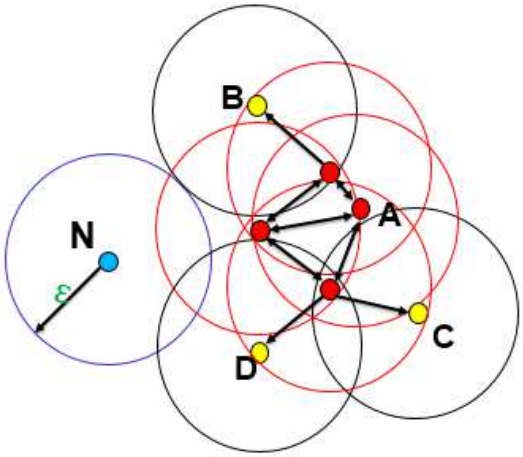

Figure 1: A schematic plot of the DBSCAN method. Given the distance ε and the parameter $M_p=3$, the red points denote core particles, because there exist at least 3 neighbor particles within the shell of size ε. The red points are connected by double-directional arrows to indicate that they are inter-connected core particles. The red points form the cluster core. The points B, C and D are not core particles, but are directly reachable from at least one red point (as indicated by the one-directional arrows). They form the boundary of the cluster. The region covered by the red circle is viewed as a clusters, because the particles in it either belong to cluster core, or are directly reachable from the cluster core. The point N is a outlier.

The DBSCAN method defines the *core particle*: a particle i is a core particle if there exist at least M_p neighboring particles in the set $\mathcal{N}(i):=\{j|d_{ij}\leq\varepsilon\}$, i.e. the number of particles in set $\mathcal{N}(i)$ is equal to or larger than M_p. A particle j is called to be *directly reachable* from i, if i is a core particle and $d_{ij}\leq\varepsilon$. Two core particles i and j are *inter-connected core particles*, if there exist a chain of core particles $x_{p_1},x_{p_2},\cdots,x_{p_m}$ satisfying $i=p_1$, $j=p_m$ and $d_{p_\alpha,p_{\alpha+1}}\leq\varepsilon$ for any $1\leq\alpha<m$. The *cluster core* is defined to be the a subset of D, in which all particles are the inter-connected core particles. The *cluster* is defined to the set formed by the cluster core and all particles directly reachable from any particle in the cluster core. The particles that are not directly reachable from any core particle are *outliers*. See Fig. 1 for a schematic illustration. The particle belonging to clusters are of solid-rich dense phase, while the outliers are of gas-rich phase.

Remark 3.1. The cores of clusters are uniquely defined, however, the "boundaries" of clusters, which do not belong to any cluster core but are directly reachable from a cluster core, is subject to ambiguity: there may exist a boundary particle that is directly reachable from two core particles that are belonging to two different cluster cores. In this case, the boundary particle is arbitrarily assigned to any of the clusters.

The DBSCAN method view clusters as regions of high density separated by regions of low density. There are two tunable parameters in this method, ε and M_p. A higher density is necessary to form a cluster if M_p is set higher or ε is set smaller, and on the other hand, a lower density is needed if M_p is set lower or ε is set larger.

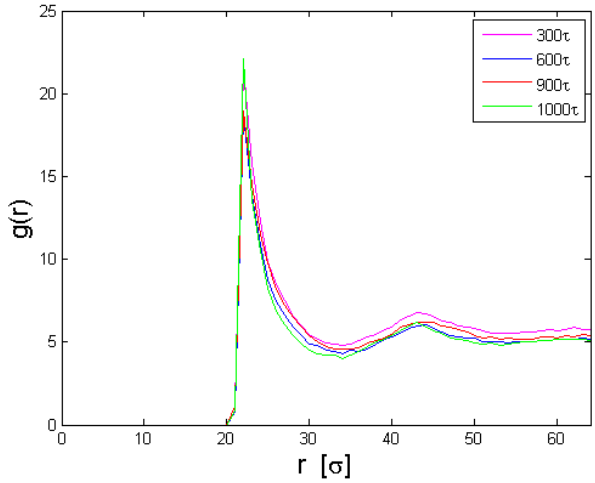

Figure 2: The radial distribution function (RDF) of the particles in solid-rich phase for the DNS data. The different colors denote the RDFs at 300τ, 600τ, 900τ and 1000τ, respectively. The RDF does not converge to 1, because the system is heterogeneous, and the investigated range $0\sigma \leq r \leq 64\sigma$ is much smaller than the typical length scale of the clusters.

To avoid the arbitrariness in the cluster identification result due to the choice of the method parameters, we determine the parameters from the intrinsic structure of the particle data to be analyzed.

For the DNS data, firstly a few representative frames are taken from the trajectory of the numerical simulation. Then the particles in the representative frames are divided in solid-rich and gas-rich phases by the method proposed by Liu et al. [9]. The radial distribution function (RDF) $g(r)$, which measures the normalized number of particles in a neighbor shell locating at r, is calculated from the solid-rich phase particles, see Fig. 2. Two peaks of $g(r)$ locating at around $r = 22\sigma$ and $r = 43\sigma$ are observed from the investigated range $0\sigma \leq r \leq 64\sigma$. They corresponds to the center of the first and second neighbor shells of the solid rich phase, respectively. Between the first and second peaks of $g(r)$, a valley is observed at about $r = 33\sigma$, which indicates the boundary between the first and second neighbor shells. It is worth noting that the location of the neighbor shell centers and the boundary between the neighbor shells does not change significantly during the simulation. According to these observations from the RDF, we investigate the local density of a particle by the range up the first neighbor shell, and set the parameter ε to the position of the valley between the first and second neighbor shell, i.e. 33σ. The numbers of neighbors in the first neighbor shell at time 300τ, 600τ, 900τ and 1000τ are 9.78, 9.75, 9.93 and 10.93, respectively. A reasonable choice of M_p is thus 10. In the next section, it will be shown that the statistics of the clusters is not sensitive to the choice of M_p if it is set around the average number of neighbors in the first neighbor shell.

For the EMMS-DPM data, the approach to determine the tunable parameters ε and M_p is the same as the DNS data. We choose three representative frames at 32.28s, 32.44s,

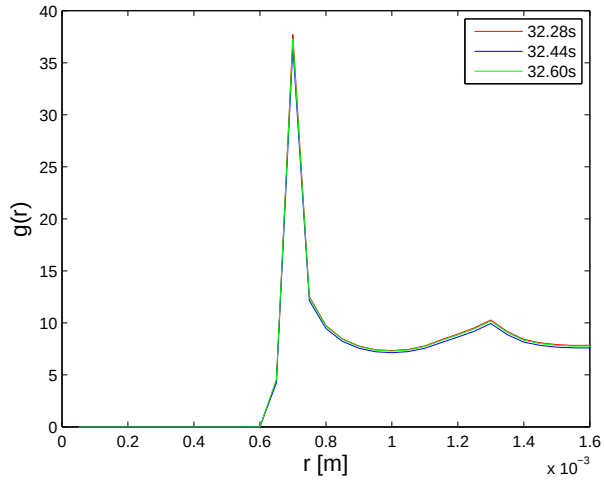

Figure 3: The radial distribution function (RDF) of the particles for the EMMS-DPM data. The different colors denote the RDFs at $32.28s$, $32.44s$ and $32.60s$, respectively.

and $32.60s$ and present the corresponding RDFs in Fig. 3. From the figure, it is observed that the RDF curves of the representative frames almost coincide with each other, and the location of the first and second neighbor shells and the boundary between the neighbor shells does not change significantly during the simulation. Thus, we set the parameter ε to the position of the valley between the first and the second neighbor shell, i.e. $1\times10^{-3}m$. The other parameter $M_p=6$ is chosen as the average number of neighbors in the first neighbor shell.

Remark 3.2. To determine the method parameters ε and M_p, we needs to analyze only a few representative snapshot on the trajectory, rather than the whole trajectory. If the simulation protocol is changed, i.e. the particle diameter and the fluid properties are changed, the model parameters should be recalibrated from the new simulation trajectories.

4 Cluster identification results

4.1 DNS particle trajectory

By the algorithm described above, we analyze all the DNS particle trajectory from τ to 1000τ and get the states of clusters at all the moments. The cluster identification results of several representative moments are shown in Fig. 4 with M_p set to 10. The domain thickness is very small compared with the domain height and width, thus the states projected to the x-y plane are shown. The time evolution of the number of clusters is reported by the red line in Fig. 6. In the Fig. 4, the outliers are not plotted, and the particles belonging to the same cluster are presented by the same color. At the beginning, all the

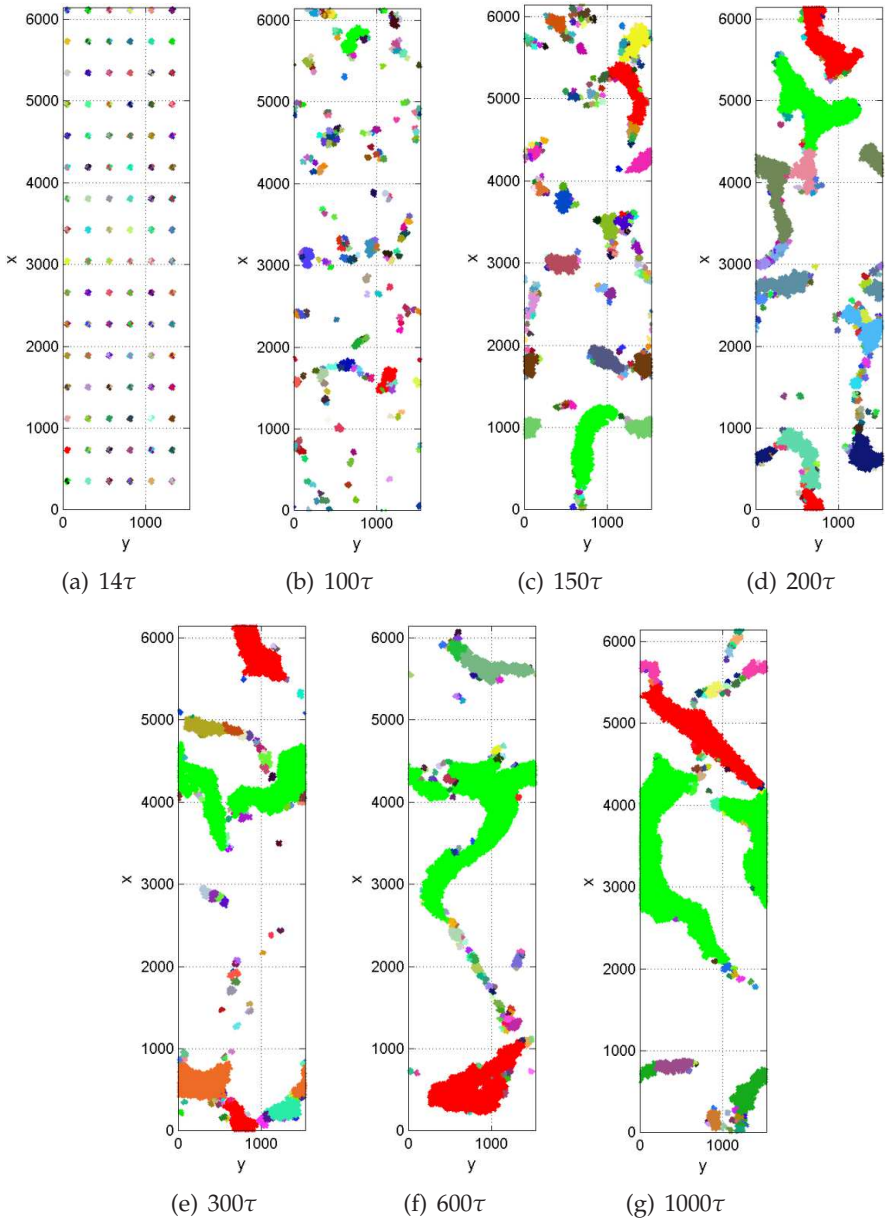

(a) 14τ (b) 100τ (c) 150τ (d) 200τ

(e) 300τ (f) 600τ (g) 1000τ

Figure 4: The clusters detected by our method at several representative moments. The green and the red regions represent the two clusters with largest sizes. The size of a cluster is counted by the number of particles belonging to that cluster.

particles in the simulation region are randomly distributed and no cluster forms. Then, as is shown in Fig. 4(a), particles form small clusters and each cluster is far apart from each other. Clusters larger than 50 are rarely observed before 100τ, see Fig. 6. Then, from 100τ to 300τ, the clusters begin to combine and split and the size of clusters increases

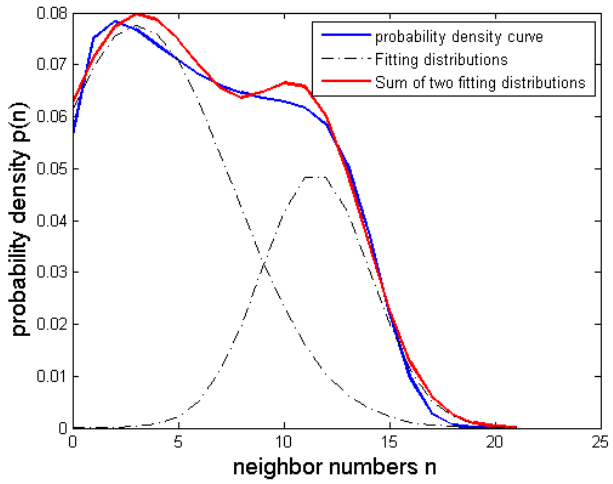

Figure 5: The probability density function of the number of near neighbors ($d_{ij} \leq \varepsilon$) at the steady state (blue line). The red line presents a bimodal fitting to the probability density function. The two modes are presented by gray dashed lines.

significantly, as is shown from Fig. 4(b) to Fig. 4(e). After 300τ, although the shape of the large clusters varies significantly, see Figs. 4(e) to 4(g), the number of clusters qualitatively does not change with time, so the system reaches a steady state, see Fig. 6. It is noted that the size of very large clusters (size larger than 10^4 is observed) is comparable to the total number of particles in the system, therefore, the behavior of these clusters is subject to the finite size effect of the simulation region.

The steady distribution of the number of near neighbors, i.e. the number of neighbors in the set $\mathcal{N}(i) = \{j | d_{ij} \leq \varepsilon\}$, is presented in Fig. 5. The distribution is estimated by averaging all available snapshots of the system in the time interval $[301\tau, 1000\tau]$. It is a bimodal distribution that can be approximately fitted with double-Gaussian distribution centering at 3.1 and 11.5 with standard deviations of 4.6 and 2.6, see the dashed lines in Fig. 5. The two modes in the distribution corresponds to the gas-rich and solid-rich phases, respectively. It is noted that the parameter M_p can also be determined by the mean of the solid-rich mode. We will show that the cluster identification result is not sensitive to the parameter M_p in range 10 to 12, thus we fix M_p to 10 in this work.

In Fig. 6, the cluster identification results with different choices of M_p is presented and compared by lines with different colors. It is observed that the number of relatively large clusters is not sensitive to M_p. After time 300τ, the numbers of clusters computed by different choices of M_p are in satisfactory consistency. Therefore, the statistics of the clusters in the steady state is not sensitive to the parameter M_p if it is set to a number around the average number of particles in the first neighbours shell. The cluster identification approach proposed by this work captures the essential phenomena of clusters in the steady state of a particle-fluid system.

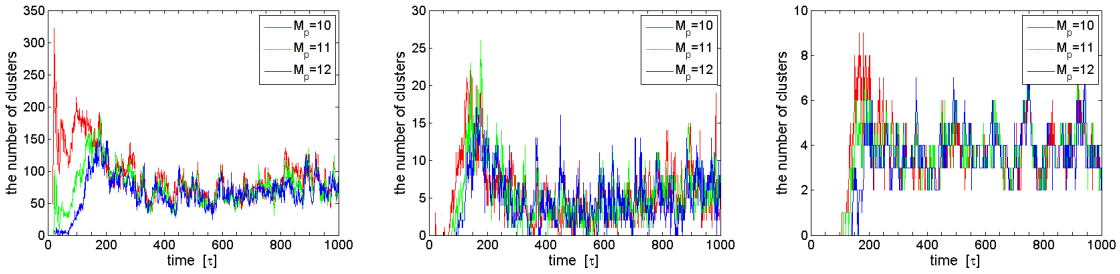

(a) clusters smaller than 50 (b) cluster size 50-500 (c) clusters larger than 500

Figure 6: The number of clusters of different sizes against time. The plots (a)-(c) show the number of clusters formed by less than 50 particles, 50-500 particles and more than 500 particles, respectively. The red, green and blue lines denote the number of clusters computed with $M_p = 10$, 11 and 12, respectively.

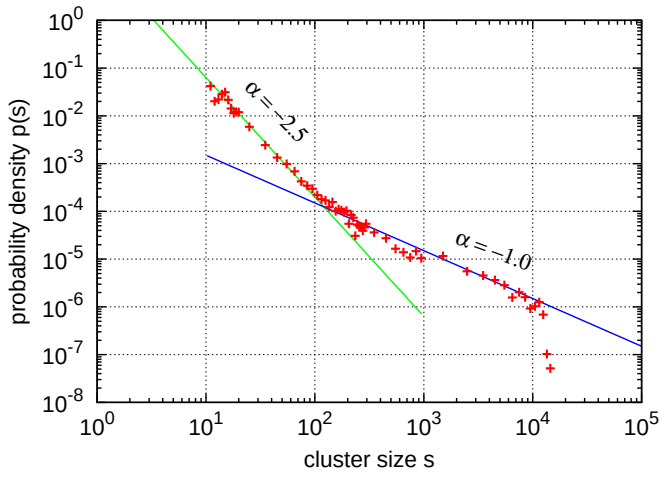

Figure 7: The probability density function $p(s)$ of the cluster size s at the steady state for the DNS data. The size of a cluster is counted by the number of particles belonging to that cluster. $p(s)$ is piecewisely fit to power laws, and the fittings on the log-log plot are presented by straight lines with the slops presented along with the lines.

The steady distribution of the cluster size is presented in Fig. 7. The distribution is computed by averaging over the time interval 301τ to 1000τ, when the system reaches the steady state. Below size 9, the definition of cluster is artificial, because the minimal size of cluster formed in gas-rich phase is limited to 10 by setting M_p to 10, and the cluster of size smaller than M_p can only form at the boundary of large clusters. Thus the clusters of size smaller than 10 are not presented in Fig. 7. It is observed from the figure that the distribution of cluster sizes follows two power laws, which are written in a unified expression as

$$p(s) \propto s^{\alpha}, \tag{4.1}$$

where s is the size of the cluster. From size 10 to 110 the distribution is fit to $\alpha=-2.5$, as indicated by the green line in Fig. 7. Larger than size 110, the population of clusters decays much slower with respect to cluster size, and the distribution $p(s)$ fits to $\alpha=-1$, as is shown by the blue line in Fig. 7. The distribution saturates after $s=10^4$, a value that is close to the number of particles (2.88×10^4) in the system.

It has been demonstrated by Ding and Aidun [3] that in a particle-fluid system, the steady distribution of cluster size follows the power law, i.e. $\propto s^{-2.5}$, in 3-dimensional space, when the cluster size is relatively small and the particles are hard and interacting hydrodynamically. Moreover, this relation is independent with the particle shape and the number of particles in the system up to the critical concentration. Our result is in perfect consistency with that reported by Ding and Aidun [3], when the cluster size is smaller than 110. The second power-law $\alpha=-1$ is caused by the limited size of the region in the z direction, which is only 128σ and is much smaller than those of the x and y directions, i.e. 6144σ and 1536σ, respectively. We find that when the size of cluster s reaches about 100, the maximum distance in z-direction between two particles in the cluster is comparable to 120σ. Thus, the cluster formation below size 110 is three-dimensional (3D) and the cluster formation above size 110 is two-dimensional (2D). The fit power law of 2D clusters ($\alpha=-1$) is larger than 3D clusters ($\alpha=-2.5$), because the surface-to-volume ratio of 2D clusters is lower, which encourages the cluster formation.

4.2 EMMS-DPM particle trajectory

We identify the clusters along the EMMS-DPM particle trajectory, and present the distribution of cluster size in Fig. 8. The distribution is computed by averaging over the time

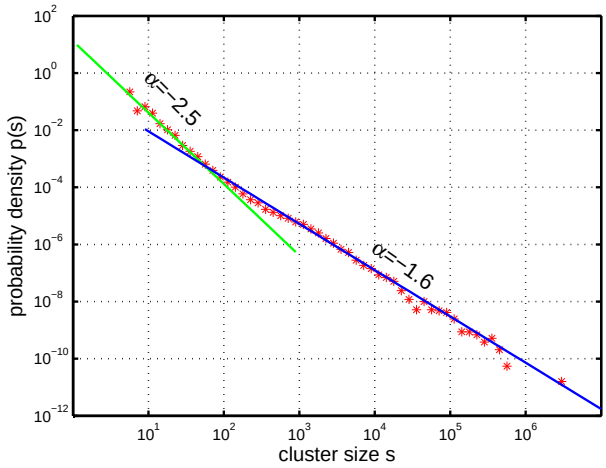

Figure 8: The probability density function $p(s)$ of the cluster size s. The size of a cluster is counted by the number of particles belonging to that cluster. $p(s)$ is piecewisely fit to power laws, and the fittings on the log-log plot are presented by straight lines with the slops presented along with the lines.

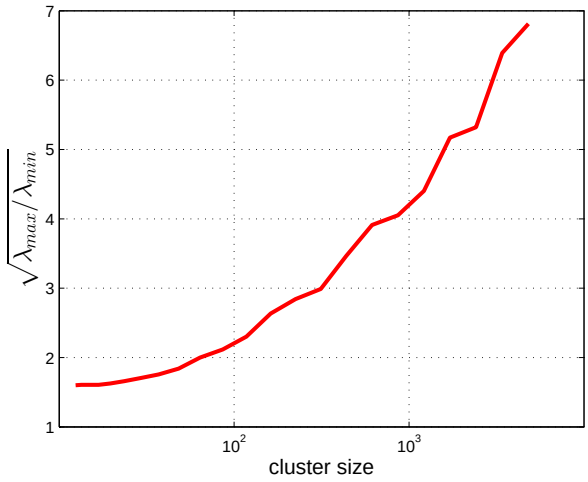

Figure 9: The square root of the ratio of maximum to minimum eigenvalues ($\sqrt{\frac{\lambda_{\max}}{\lambda_{\min}}}$) of shape matrix against cluster size. The size of a cluster is counted by the number of particles belonging to that cluster.

interval 32.28s to 32.60s, and the clusters smaller than 6 are not presented. The distribution of cluster sizes follows two power laws. From size 6 to $\sim$78, it fits to $\alpha=-2.5$, which is identical to the DNS particle trajectory, and that reported by Ding and Aidun [3], as is shown by the green line in the figure. From size $\sim$78 to 10^7, the distribution fits to $\alpha=-1.6$, which decays faster than the DNS particle trajectory ($\alpha=-1.0$), as is shown by the blue line in the figure.

To analyze the shape of the clusters, we introduce the shape matrix that describes the shape of the clusters

$$\begin{bmatrix} \int x^2 dm & \int xy dm & \int xz dm \\ \int xy dm & \int y^2 dm & \int yz dm \\ \int xz dm & \int yz dm & \int z^2 dm \end{bmatrix}. \tag{4.2}$$

The maximum and the minimum eigenvalues of the shape matrix (4.2) are denoted by $\lambda_{\max}$ and $\lambda_{\min}$, respectively. The value $\sqrt{\lambda_{\max}/\lambda_{\min}}$ describes how far the shape of the cluster deviates from a sphere. This can be seen by assuming the mass distribution of a cluster satisfies the 3-dimensional Gaussian distribution, then the value $\sqrt{\lambda_{\max}/\lambda_{\min}}$ is equal to the ratio of the long axis to the short axis of the ellipsoidal isosurfaces. In this work, we say that a cluster is not spherical like when $\sqrt{\lambda_{\max}/\lambda_{\min}}>2$. In Fig. 9, the value $\sqrt{\lambda_{\max}/\lambda_{\min}}$ is presented for clusters sizes ranging from 10 to 5000. It is observed that when the cluster size reaches 81, then cluster is not spherical like. This is in a good agreement with the cross-over between the power laws $\alpha=-2.5$ and $\alpha=-1.6$. It is indicated that when the cluster size is larger than 81, the growth of cluster is not in a 3D spherical way, and the cluster shape starts to be affected by the cylindrical simulation region, which effectively encourages the formation of clusters.

5 Conclusion

In this paper, a cluster identification method based on DBSCAN is proposed to identify the clusters in the particle-fluid systems. The characteristics of our methods are:

- Only the particle position is used for clustering, while neither gas velocity nor particle velocity is used.
- The parameters ε and M_p in the DBSCAN method are determined by analyzing the structure of particle information in a few snapshots, thus the human intervention is minimized.
- The method can identity the dilute and dense phase automatically. We don't need to calculate the porosity of each particle and determine a threshold to identify the dilute and dense phase.
- The number of clusters don't need to be specified before analyzing.
- All kinds of cluster shapes can be attained by this method.
- The complexity of the algorithm is $\mathcal{O}(N\log N)$ [4] with N being the number of particles in the system.

The method is illustrated by analyzing the DNS simulation trajectories from Zhou et al. [17] and the EMMS-DPM simulation trajectories from Ji Xu et al. For the DNS data, we show that the system reaches the steady state after 300τ. The steady distribution of the cluster size can be fit to two power laws with exponents $\alpha=-2.5$ and -1 when the cluster size is smaller than 110 and larger than 110, respectively. Besides, for the EMMS-DPM data, the distribution of cluster size can also be fit to two different power laws with exponents $\alpha=-2.5$ and -1.6 in the regions where the cluster size is smaller and larger than 78, respectively. The results above all correctly reproduce the cluster distribution power law $s^{-2.5}$ for relatively small clusters reported in literature. Besides, the cluster size distributions of the two systems all satisfy two different power law functions in two different cluster-size regions, which is caused by the size effect of the simulation region. It is noted that our clustering method is based on rigid mathematical criteria, and the good agreement with power-law behavior of the cluster size distribution reported in the literature stimulates further investigations on the other properties of the clusters.

Acknowledgments

The authors gratefully acknowledge financial support from the National Natural Science Foundation of China grant Nos. 91434201, 11421101 and Key Research Program of Frontier Sciences, China Academy of Sciences grant No. QYZDJ-SSW-JSC029, the data from Ji Xu et al. and Guofeng Zhou et al., and the help from Limin Wang and Xiaowen Liu.

References

[1] A. Cahyadi, A. Anantharaman, S. Yang, S. B. R. Karri, J. G. Findlay, R. A. Cocco, and J. W. Chew. Review of cluster characteristics in circulating fluidized bed (CFB) risers. *Chemical Engineering Science*, 158:70–95, 2017.

[2] P. A. Cundall and O. D. L. Strack. A discrete numerical model for granular assemblies. *Geotechnique*, 29(1):47–65, 1979.

[3] E-J. Ding and C. K. Aidun. Cluster size distribution and scaling for spherical particles and red blood cells in pressure-driven flows at small Reynolds number. *Physical Review Letters*, 96(20):204502, 2006.

[4] M. Ester, H.-P. Kriegel, J. Sander, X. Xu et al. A density-based algorithm for discovering clusters in large spatial databases with noise. In *KDD*, 96:226–231, 1996.

[5] J. Li and W. Huang. From multiscale to mesoscience: Addressing mesoscales in mesoregimes of different levels. *Annual Review of Chemical and Biomolecular Engineering*, 9:41–60, 2018.

[6] J. Li. *Particle-Fluid Two-Phase Flow: The Energy-Minimization Multi-Scale Method*. Metallurgical Industry Press, 1994.

[7] J. Li and M. Kwauk. Multiscale nature of complex fluid-particle systems. *Industrial & Engineering Chemistry Research*, 40(20):4227–4237, 2001.

[8] J. Li, Y. Tung, and M. Kwauk. Method of energy minimization in multi-scale modeling of particle-fluid two-phase flow. In *Circulating Fluidized Bed Technology: Proceedings of the Second International Conference*, pages 89–103. Elsevier, 1988.

[9] X. Liu, L. Wang, and W. Ge. Meso-scale statistical properties of gas-solid flow — a direct numerical simulation (DNS) study. *AIChE Journal*, 63(1):3–14, 2017.

[10] G. R. McNamara and G. Zanetti. Use of the Boltzmann equation to simulate lattice-gas automata. *Physical Review Letters*, 61(20):2332, 1988.

[11] C. S. Peskin. Flow patterns around heart valves: A numerical method. *Journal of Computational Physics*, 10(2):252–271, 1972.

[12] L. Reh. New and efficient high-temperature processes with circulating fluid bed reactors. *Chemical Engineering & Technology*, 18(2):75–89, 1995.

[13] A. K. Sharma, K. Tuzla, J. Matsen, and J. C. Chen. Parametric effects of particle size and gas velocity on cluster characteristics in fast fluidized beds. *Powder Technology*, 111(1-2):114–122, 2000.

[14] C. H. Soong, K. Tuzla, and J. C. Chen. Identification of particle clusters in circulating fluidized bed. *Circulating Fluidized Bed Technology*, 4:615–620, 1994.

[15] K. Tuzla, A. K. Sharma, J. C. Chen, T. Schiewe, K. E. Wirth, and O. Molerus. Transient dynamics of solid concentration in downer fluidized bed. *Powder Technology*, 100(2-3):166–172, 1998.

[16] J. Xu and J. Zhu. A new method for the determination of cluster velocity and size in a circulating fluidized bed. *Industrial & Engineering Chemistry Research*, 51(4):2143–2151, 2011.

[17] G. Zhou, Q. Xiong, L. Wang, X. Wang, X. Ren, and W. Ge. Structure-dependent drag in gas-solid flows studied with direct numerical simulation. *Chemical Engineering Science*, 116:9–22, 2014.

[18] J.-X. Zhu and H.-T. Bi. Distinctions between low density and high density circulating fluidized beds. *The Canadian Journal of Chemical Engineering*, 73(5):644–649, 1995.